Journal of Materials Chemistry A

ROYAL SOCIETY OF CHEMISTRY

PAPER

View Article Online
View Journal | View Issue

Cite this: J. Mater. Chem. A, 2023, 11, 20129

Bridging the gap between basic research and application: a half-cell setup for high current density measurements of Ir-based oxygen evolution reaction catalysts on porous transport electrodes†

Pablo Collantes Jiménez, [a] Gustav K. H. Wiberg, [b] Gustav W. Sievers, [a] Volker Brüser[a] and Matthias Arenz *[b]

Electrochemical benchmarking in three-electrode setups at a laboratory scale can greatly accelerate the development of catalysts for the oxygen evolution reaction in proton exchange membrane water electrolyzers. However, current systems such as the rotating disk electrode suffer from measurement artifacts, low current densities, and limited extrinsic validity. In this study, we introduce a novel three-electrode setup referred to as the PTE setup, specifically designed to investigate OER catalysts on realistic porous transport electrodes (PTEs) used in the anode side of water electrolyzers at high current densities. We evaluated the effectiveness of the PTE setup using self-supported iridium oxide (IrO_x) and Ir–Co catalysts produced *via* physical vapor deposition on a porous Ti porous transport layer (PTL) and pressed to a Nafion membrane. Our results demonstrate that the PTE setup is capable of measuring the activity and stability of self-supported catalysts creating conditions found in the anode cell compartment of a single-cell electrolyzer at current densities up to 2 A cm_{geo}^{-2}. This setup represents a promising alternative to traditional benchmarking techniques, offering a practical and efficient approach for evaluating catalyst performance in relevant electrochemical environments.

Received 13th July 2023
Accepted 6th September 2023

DOI: 10.1039/d3ta04136k

rsc.li/materials-a

1. Introduction

Optimizing efficiency and reducing the consumption of critical raw materials in electrocatalysts is of paramount importance to achieve a significant increase in hydrogen production.[1,2] Hence, bridging catalyst research into their application is of prime interest. With respect to proton exchange membrane water electrolyzers (PEMWEs), for their large-scale commercialization, testing oxygen evolution reaction (OER) catalysts at high current densities is essential. Such testing should not be limited to activity measurements but also needs to include accelerated stress tests. To date, most activity and degradation studies start with half-cell studies in rotating disk electrodes which are later verified in membrane electrode assembly techniques, which effectively work as single cells.[3–12] In this regard, the gap between model studies and application is large. In single-cell tests, focusing on the anode catalyst degradation behavior can be challenging due to the overlapping effects with other cell elements. At the very least, full-scale trials are material and time-intensive processes, which rely on a series of instruments and stack engineering not available to every research group. On the other hand, while the rotating disk electrode technique is very useful for fundamental studies of intrinsic catalyst activities, it falls short of representing relevant electrode morphologies and their mass transport behavior under realistic operating conditions.[7,9,13,14] Furthermore, the lack of mass transport in liquid electrolyte compared to membrane assemblies limits the achievable current densities to less than 100 mA cm_{geo}^{-2}.[15] For accelerated stress test studies and catalyst dissolution rate measurements, flow cells are the state-of-the-art laboratory setups for online spectrometry such as in-coupled spectroscopy studies.[16,17] However, the direct contact of the electrolyte with the catalyst surface also leads to a substantial overestimation of the catalyst dissolution rates as compared to accelerated stress tests in membrane electrode assemblies[18] Hence, stability data obtained from aqueous systems have to be interpreted carefully. Alternatively, the recently developed gas diffusion electrode (GDE) half-cell setup offers a more accurate physical representation of the individual electrode reactions due to its three-electrode configuration

[a]Leibniz Institute for Plasma Science and Technology, Felix-Hausdorff-Strasse 2, 17489, Greifswald, Germany. E-mail: sievers@inp-greifswald.de; matthias.arenz@unibe.ch

[b]Department of Chemistry, Biochemistry and Pharmaceutical Sciences, University of Bern, Freiestrasse 3, CH-3012 Bern, Switzerland

† Electronic supplementary information (ESI) available. See DOI: https://doi.org/10.1039/d3ta04136k

while preserving the fast screening and flexibility that is desired for laboratory techniques. In particular, a key feature of the GDE setup is the ability to perform realistic electrode preparation processes, which unlike in rotating disk electrode measurements, permits the study of the triple phase boundary of catalyst layers. By hot-pressing the coated substrate with a proton exchange membrane, the catalyst performance can be studied at high-current densities without limitations in gas solubility and bubble formation in liquid electrolyte.[6] While the GDE technique has been featured primarily in ORR studies using carbon gas diffusion layers,[19–22] recent efforts have been made to allow their application in OER studies for Ir-supported catalysts to match previous rotating disk electrode studies.[23,24] However, the high positive potentials required for the OER accelerate carbon corrosion,[25] which can lead to flooding due to changes in the gas diffusion layer hydrophobicity. Under these conditions, the current is unevenly distributed, resulting in early failure due to emerging "hot spots" in the membrane causing uneven swelling and detachment from the catalyst. For this reason, catalyst formulations based on carbon-supported Ir nanoparticles typically struggle with early corrosion onsets resulting in catalyst agglomeration[26,27] and loss of surface area.

On the other hand, an increased OER activity up to 10-fold higher compared to commercial catalysts has already been obtained in the former GDE setup for a new type of Ir-based self-supported catalysts with a large electrochemical surface area. This is obtained by a combined alternated magnetron sputtering and acid leaching step, eliminating the need for carbon in their composition and potentially increasing their stability.[28] Even though these catalysts demonstrated higher activity, their performance and stability measurements were initially limited due to the constraints of the GDE setup, particularly when working with carbon-based Gas Diffusion Layer (GDL) substrates. Consequently, it became essential to improve the measurement technique to perform catalyst stability measurements using Porous Transport Electrodes (PTEs) using the more chemically robust titanium (Ti) porous transport layer (PTL) substrates.

In this work, we develop the GDE setup to enable testing at industrially relevant electrolysis conditions. To this end, we optimized the electrode assembly on Ti PTLs with a magnetron-sputtered IrO_x catalyst with an 0.250 mg_{Ir} cm_{geo}^{-2} loading to minimize the influence of material-related processing steps needed for the Ir–Co catalysts. Following the first positive results in the cell configuration achieving current densities >2 A cm_{geo}^{-2} in an OER current-step protocol, we conducted a 20 h steady-state stability protocol at room temperature. The beginning-of-life and end-of-life OER activity and stability measurements, completed with cyclic voltammetry data, suggest that the new method can be used to extract meaningful information about the catalyst stability and perform degradation studies. Furthermore, the OER activity and stability of the Ir–Co self-supported catalyst sputtered on a Ti PTL with the same Ir loading and a nominal Co : Ir ratio of 4 was benchmarked and compared to the standard IrO_x in the new PTE setup. Ultimately, this study showcases the possibilities of this technique to the new generations of self-supported catalysts and the high flexibility to adapt the setup to specific conditions by performing minor changes in its configuration.[29]

2. Experimental

2.1 Materials, chemicals, gases

De-ionized (DI) ultrapure water (resistivity >18.2 MΩ cm, total organic carbon (TOC) < 5 ppb) from an Aquinity P-10^2 system (Membrapure, Germany) was used for electrolyte preparation, the cleaning of the upper cell parts and reactant in the PTE setup. Carbon gas diffusion layers with a microporous layer (Sigracet 29BC, 325 μm thick, Fuel Cell Store) served as a substrate for the sputtering of the catalyst film for the GDE preparation. Conversely, a Ti porous transport layer (PTL) (ANKURO Int. GmbH, 0.3 mm thickness, 50% open porosity) was used to create the PTEs. Polytetrafluoroethylene (PTFE) disks (Bola, 0.12 and 0.25 mm thicknesses), a gas diffusion layer without a microporous layer (Freudenberg H23, 210 μm thick, Fuel Cell Store), uncoated PTLs and Nafion membrane (Nafion 117, 183 μm thick, Chemours, Wilmington, DE, USA) were used for the cell assembly in GDE (Fig. S1†) and PTE (Fig. S2†) configurations. As a counter electrode, a platinum wire of 0.5 mm diameter (99.99%, Junker Edelmetalle GmbH) was used, which was folded several times at one side to increase the active surface area. Perchloric acid (70% HClO4, Suprapur, Merck) was used for electrolyte preparation. O_2 (99.999%, Air Liquide) and Ar (99.999%, Air Liquide) were used for magnetron sputtering, acid leaching, and electrochemical measurements.

2.2 Catalyst synthesis and electrode preparation

To prepare the self-supported IrO_x catalyst film on the carbon gas diffusion layer substrates and Ti PTL substrates, a linear sputtering magnetron reactor (Univex 400, Leybold GmbH, Germany) was used. The process chamber was evacuated to a pressure of 1.7×10^{-5} Pa. The substrate was first cleaned in acetone and isopropanol, and placed on a holder in a load lock at atmospheric pressure. Then, the chamber was evacuated to a base pressure of at least 10^{-4} Pa. From there, a swiveling arm allowed the holder to enter the process chamber with minimal interruption. To create the plasma during the deposition, an Ar and O_2 mixture with a 2 : 3 ratio was ignited at the magnetron electrode at a working pressure of 5 Pa and flushed through the individual magnetron sources at a flow rate of 100 sccm. For the IrO_x deposition, a magnetron was equipped with a planar target of Ir (99.95%, MaTecK, Germany) of 177 × 25 × 1.5 mm located at the upper part of the chamber. The RF generator (Cito 136, COMET) operated at a driving frequency of 13.56 MHz. A mask of a 5 cm × 5 cm window on the substrate holder limited the sputtered area during the deposition. The RF power was 158 W for the Ir source. The sputtering process was performed in a continuous deposition during 748 s until the desired Ir loading of 0.250 mg cm_{geo}^{-2} was reached. The Ir–Co catalyst was prepared with the same Ir loading and a nominal Co : Ir ratio of 4 as described by Collantes *et al.*,[28] except a Ti PTL substrate was used instead of a carbon gas diffusion layer. Following the deposition, the Ir–Co electrode was leached

Table 1 Electrochemical protocol used for OER and stability determination of the IrO_x catalyst in GDE and PTE setup, indicating differences in bold

Step	Electrochemical technique	Parameters	
Reference electrode calibration **(both setups)**	Open circuit potential (OCP)	Gas purge (flow rate)	H_2 (250 ml min^{-1})
		Time	~5 min
Electrochemical cleaning **(both setups)**	Cyclic voltammograms (CV)	Gas purge (flow rate)	Ar (100 ml min^{-1}), humidified
		Potential limits	0.05–1.2 V_{RHE}
		Scan rate	100 mV s^{-1}
		Number of cycles	~30 (until CV is stable)
OER activity	Galvanostatic steps coupled with online high-frequency resistance determination	Reactant supply	**GDE setup**: Ar (100 ml min^{-1}), humidified, **PTE setup**: H_2O (40 ml min^{-1})
		Current steps (hold in s)	1–2000 mA cm_{geo}^{-2}, 10 s per step, integrated potential over the last s per step (30 s per step for IrCo, integrated potential over the last 10 s per step)
		iR-correction	5 kHz, variable amplitude (100% post-correction)
Stability trial **(PTE setup)**	Galvanostatic steps coupled with online high-frequency resistance determination	Current steps (18 000 s hold)	~2 A cm_{geo}^{-2}, 4 block sequence
		iR-correction	5 kHz, 5 mV (100% post-correction)

chemically in 1 M $HClO_4$ for 30 min and then cleaned with DI water to wash any acid before pressing with the membrane. The hot-pressed procedure and assemblies for the respective GDEs and PTEs are described in detail in the ESI, see Fig. S1 and S2.†

2.3 Electrochemical measurements

All the experiments were conducted with a Potentiostat (ECi-211, Nordic Electrochemistry ApS, Denmark). An overview of the experimental protocol is presented below in Table 1.

The OER activity was determined through a quasi-steady state galvanostatic step protocol with increasing currents based on Schröder *et al.*[23] and scaled accordingly to account for the loading difference. An AC signal (5000 Hz, amplitude 1–5% of applied current) was applied during the current steps to obtain an online high-frequency resistance (HFR) measurement between the working and reference electrode, which was used for an *iR*-correction of the measured potential values.

3. Results and discussion

3.1 Setup development: from GDE to PTE

The GDE half-cell setup described by Schröder *et al.*[23] constituted a good starting point to work with carbon gas diffusion layer substrates, which were initially pressed at room temperature, *i.e.*, cold-pressed. The introduction of the hot-pressing step was a key element to stabilize the membrane assembly at higher current densities and avoid detachment due to bubble formation,[30] see Fig. 1.

While the hot pressing of the GDE was an important element in extending the kinetic-dominated potential region, mass transport limitations were still present at current densities greater than 100 mA cm_{geo}^{-2}.[28] There were further limitations due to the setup configuration, as it was previously reported by Wiberg *et al.*[29] that the position of the reference electrode and the counter electrode in the single chamber design could vary during the measurements, therefore leading to substantial differences in the *iR* correction especially at high current densities.

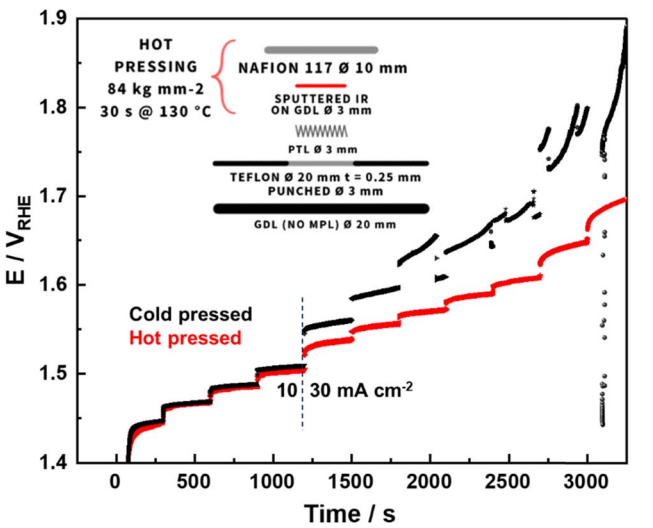

Fig. 1 Influence of hot pressing on the observed potential of a metallic Ir sputtered catalyst layer with a 1 mg cm_{geo}^{-2} loading measured in the GDE setup. The test was conducted in a galvanostatic step protocol with current densities increasing from 1, 2.5, 5, 10, 30, 45, 60, 80, 100, 150 to 200 mA cm_{geo}^{-2} in steps of 5 minutes per current density. The measurements were performed at room temperature. The black line corresponds to a cold-pressed sample, exhibiting contact problems beyond 30 mA cm_{geo}^{-2}. A hot-pressed sample, in the red line, achieved an extended current density range without showing contact problems. The inset shows a cross-section of the inner cell assembly with details of the hot pressing process.

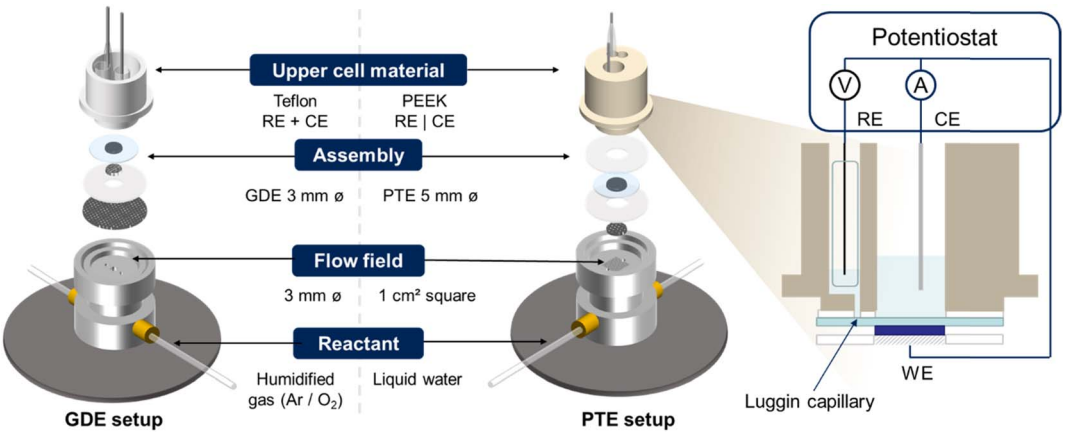

Fig. 2 Schematics of the design evolution from the GDE setup (left) to the PTE setup (center) and a detail of the cross-section of the top cell (right) showing the position of the Luggin capillary to the reference electrode (RE) compartment, the position of the working electrode (WE) and the independent chamber for the counter electrode (CE).

At the same time, given the small area of the working electrode (WE), the edge imperfections and inhomogeneities led to a larger spread in the obtained results. High current densities lead to intense bubble formation at the CE, which is easily stuck in the PTFE upper cell due to its aerophilic nature.[31,32] This can lead to a blocking of the 3 ∅ mm aperture of the PTFE cell rendering the covered areas inactive and leading to very high local currents in the adjacent areas or even a complete loss of potential control at the WE. All these effects can cause pronounced degradation effects.

Based on these observations, a new top cell was designed to test Ti PTLs. PEEK was used instead of PTFE since its comparatively lower hydrophobicity reduced the bubble adhesion. The single chamber design of the cell top part was also substituted by two independent electrolyte compartments. The main compartment cantered over the assembly was reserved for the CE. Adjacent to this, another chamber was designed for the reference electrode with a Luggin capillary. At first, the Luggin capillary ended directly over the aperture of the main compartment, but it was experimentally observed that with the two reservoirs of electrolyte in contact, the *iR* was not less than 4–5 Ohm even at low current densities where no excessive bubble formation that could affect the Luggin capillary channel is expected. Most importantly, altering the position of the counter electrode affected the measured *iR* drop. Since there should not be an electric field inside the Luggin capillary (no current through the RE), these observed variations can be attributed to a distorted electric field due to the non-ideal geometry of the working and counter electrode. Hence, in the final version of the cell, a Luggin capillary with an independent electrolyte reservoir was designed to directly probe the membrane. With this design, the *iR* drop was minimized to 0.1–0.3 Ohm and remained independent of the counter electrode position as long as the electrolyte was not transferred between the two chambers.

The contact assembly also had to be redesigned to accommodate the thicker (0.3 mm) Ti PTL, which was increased to 5 mm in diameter to offset the edge imperfections caused by the sample extraction process. Furthermore, a liquid water feed by a peristaltic pump replaced the humidified gas, and the carbon gas diffusion layer backing was discarded, thus eliminating all sources of carbon degradation. Instead, two Teflon disks were used to ensure tight sealing. To achieve a more even water flow and to minimize the plastic deformation of the membrane through the top cell apertures due to the upward pressure from the water supply and gas evolution, a bottom cell with a rectangular flow field pattern was used. The combination of all these improvements on the former GDE setup resulted in the PTE setup displayed in Fig. 2.

3.2 Parametric study in the PTE setup

A comparative series of OER activity measurements was performed in the PTE setup using carbon gas diffusion electrodes (GDEs) and Ti porous transport electrodes (PTEs) with an IrO_x catalyst with 0.250 mg_{Ir} cm_{geo}^{-2}, see Fig. 3A. After deposition, a homogeneous catalyst layer was found even on the highly porous Ti PTL fibers, see the cross-section in Fig. 3B and C. Using IrO_x as a benchmark allowed us to concentrate the characterization efforts on evaluating the impact of substrate type, reactant supply, and hot-pressing configurations. This approach eliminates the requirement for additional processing steps such as acid leaching or activation necessary for Ir–Co catalysts.

Considering the data series hot pressed at 84 bar (red) in Fig. 3A, using liquid water in GDE assemblies (filled red circles) resulted in a slightly poorer performance already at low current densities as compared to the GDEs supplied with humidified gas (hollow red circles), indicating flooding problems.

The latter was still better than PTE assemblies under the same conditions (hollow red triangles), which could be expected from the larger pore structure at the surface in the PTEs, not optimized to maximize the number of active sites. Regardless, the trend in all series was to experience very high with very noticeable after 100 mA cm_{geo}^{-2} due to diffusion limitations from the humidified gas together with the instability of carbon

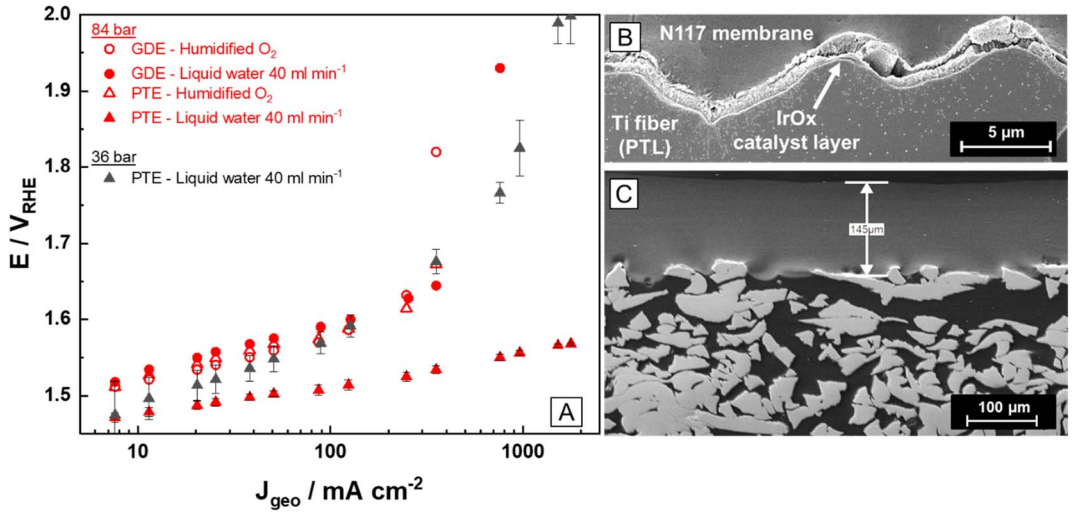

Fig. 3 (A) Influence of the configuration of the substrate (GDEs *vs.* PTEs), the supply of reactant (humidified O_2 *vs.* liquid water), and the hot-pressing (36 *vs.* 84 bar) in the OER activity of a sputtered IrO_x 0.250 mg cm_{geo}^{-2} catalyst measured in the PTE setup. The best setup, substrate, and reactant supply combination produced an OER activity of ~1.57 V_{RHE} at 2 A cm_{geo}^{-2}. (B) Cross-section micrograph obtained by scanning electron microscopy of the PTE before OER showing a homogeneous IrO_x layer thickness. (C) A wider view of the cross-section of the electrode where the interfaces in contact with the fibers and membrane, internal porosity as well as membrane thickness are visible.

degradation particularly in the GDE assemblies. On the other hand, a radically different behavior was observed when combining PTEs with liquid water, reaching current densities up to 2 A cm_{geo}^{-2} (filled red triangles) at 1.55 V_{RHE}. This is a noticeable improvement as compared to the previous study designs, where the current was limited to around one order in magnitude lower values.[23] Next, the influence of the pressure applied during hot pressing of the PTEs over the OER activity was studied as several studies have reported that high pressures applied to the stiff Ti PTL fibers can accelerate pinhole formation in the membrane and reduce the catalyst efficiency due to gas crossover or cause short circuits.[33,34] This was a relevant concern in the context of this study where a larger weight was needed to maintain the pressure conditions with 5 ∅ mm samples. Hence, the OER performance using liquid water was measured for another three PTEs hot-pressed at a lower pressure of 7 kgf (~36 bar) and compared to the nominal 16.6 kgf (~84 bar). The low-pressure settings (filled black triangles) circles consistently lead to increased overpotentials already at relatively low current densities and large concomitant Tafel slopes (80–100 mV dec^{-1}) when going to medium current densities and beyond, see Fig. 3A. In contrast, the PTEs hot-pressed at 84 bar (filled red triangles), exhibited substantially improved and more reproducible activity results to the point where the error bars are barely visible over the averaged data. Within this series of measurements, a Tafel slope of 37 mV dec^{-1} was calculated in the 10–50 mA cm_{geo}^{-2} region, see Table 2. Interestingly, with *iR* correction, a linear Tafel of 42 mV dec^{-1} could still be extracted when increasing the upper fitting threshold to 2 A cm_{geo}^{-2} currents, indicating minor or no diffusion limitations. In summary, the GDE setup shows no substantial differences between the use of humidified gas and water for either substrate, while in the PTE setup, the current density using humidified gas or low pressing conditions remains low. Hence, it can be concluded from these experiments that the only way to enable high current densities is by using PTEs with liquid water in the high hot-pressure setting in combination with the PTE setup. A summary of the relevant electrochemical findings can be seen in Table 2.

Table 2 Summary of the influence of different study parameters in the Tafel behavior and OER current density measured at 1.55 V_{RHE} of an IrO_x 0.250 mg cm_{geo}^{-2} catalyst sputtered both on carbon gas diffusion layers (GDLs) and Ti porous transport layers (PTLs)

Setup configuration	Substrate type	Reactant type	Hot pressing pressure (bar)	Tafel slope@10–50 mA cm_{geo}^{-2} (mV dec^{-1})	Current density (mA cm_{geo}^{-2})@1.55 V_{RHE}
GDE setup[a]	Carbon GDL	Humidified gas (O_2)	84	70	21.4
PTE setup	Carbon GDL	Humidified gas (O_2)	84	57	36.5
		Liquid water (40 ml min^{-1})	84	68	20.6
	Ti PTL	Humidified gas (O_2)	84	67	27.0
		Liquid water (40 ml min^{-1})	**84**	**37**	**758.7**
			36	93	50.8

[a] Represented in Fig. S2 in the ESI, section "Setup reproducibility".

3.3 Stability tests

After successfully reaching high current densities without noticeable mass transfer limitations in the polarization curves performed in the PTE setup, a longer stability test was designed to resemble operation conditions seen in membrane electrode assemblies. Previous studies report that the most demanding conditions for anode catalyst stability are met at continuous high-current density tests with an extended duration.[5,8,15,35] Using the IrO_x catalyst as a benchmark for the proposed protocol, a constant current density of 2 A cm_{geo}^{-2} was applied for 20 h, separated into 4 sequenced blocks of 5 h. The HFR was measured online using an AC signal at 5 kHz and 5 mV amplitude, which allowed the continuous measurement of the cell resistance while minimally disturbing the measurement. During the first five hours of the stability measurement, the *iR*-free electrode potential, represented in black in Fig. 4A, remained stable with only local fluctuations during the conditioning in the first hour as well as an upward jump at the end of the period. Small disturbances in the range of a few tenths of mV were always present due to temporary gas bubble formation at the Pt CE. The readout time of the protocol macro in the Potentiostat produced a 1 or 2 second-long OCP period between the blocks where the activity of the catalyst was recovered in a downward jump, an effect also seen in membrane electrode assembly configurations.[35,36] The HFR, see Fig. 4B, was initially very low at approx. 100 mOhm, and only experienced a slight increase up to approx. 150 mOhm during the first 5 hour period. In later blocks, high potential intervals appeared during short times.

These interferences, which are also visible in the HFR resistance measurement, correspond to temporary blockages of the Luggin capillary. Even though the blocked reference electrode prevented the direct interpretation of the degradation from the potential trend, the measurement remained valid as the current was still applied continuously, see the right axis in Fig. 4A.

As the measurement progressed, the cell resistance plotted in black in Fig. 4C showed a steep increase during the measurement until a cell potential of 10 V was reached. A further inspection of the cell chambers after the test revealed that the main chamber was almost fully empty of electrolyte. During the measurement, the fast evolution of H_2 bubbles on the Pt wire at the counter electrode could have caused the electrolyte to evaporate faster, lowering the area in contact with the electrode and continuously increasing the cell resistance. In the last 5 hour period, the 10 V compliance voltage of the Potentiostat was reached altering the correct recording of the HFR-free voltage data, see the red dotted line in Fig. 4B. After the test, the cell was refilled with electrolyte and the reversible hydrogen electrode was remade to eliminate any offsets.

In the next step, the stability of an Ir–Co catalyst sputtered on a Ti PTL substrate was compared to that of the IrO_x in a short 5 hour measurement stability measurement at 2 A cm^{-2} and 60 °C, see inset in Fig. 4A. The graph shows a reduced number of data points for a more clear comparison. Aside from an expected decrease of *ca.* 25 mV in the reversible electrode potential from the temperature difference, the further reduction would support the effects of an activation process observed in this type of catalyst.[28] Notably, it was also possible to record a stable potential with this material even at 60 °C where a lower stability could have been expected in comparison to the IrO_x benchmark measured at RT. The catalyst degradation produced in the stability measurement was assessed by performing cyclic voltammetry and OER activity measurements in beginning-of-life and end-of-life states, see Fig. 5.

For the IrO_x catalyst, the degradation can be interpreted from the decrease (6 mV dec^{-1}) in the Tafel slope between beginning-of-life and end-of-life OER activity, see Fig. 5A. Additionally, two 30 minute potential intervals from the

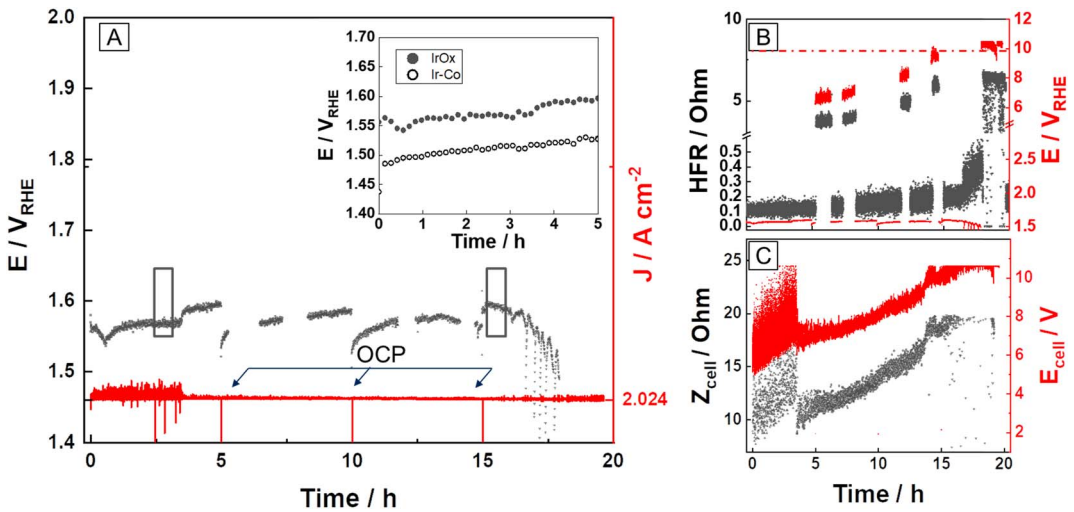

Fig. 4 (A) Stability measured at room temperature on the PTE setup of a 0.250 mg_{Ir} cm_{geo}^{-2} IrO_x catalyst sputtered on Ti PTL. For comparison, the inset in the graph shows the stability of the 0.250 mg_{Ir} cm_{geo}^{-2} Ir–Co catalyst measured at 60 °C in a 5 h period. (B and C) Show a cross-examination of measurement signals to determine the origin of the high potential regions during the stability IrO_x catalyst. (B) HFR (left axis) and HFR-free voltage (right axis) *vs.* time. The dotted line indicates the compliance voltage limit. (C) Cell resistance (left axis) and cell potential (right axis) *vs.* time.

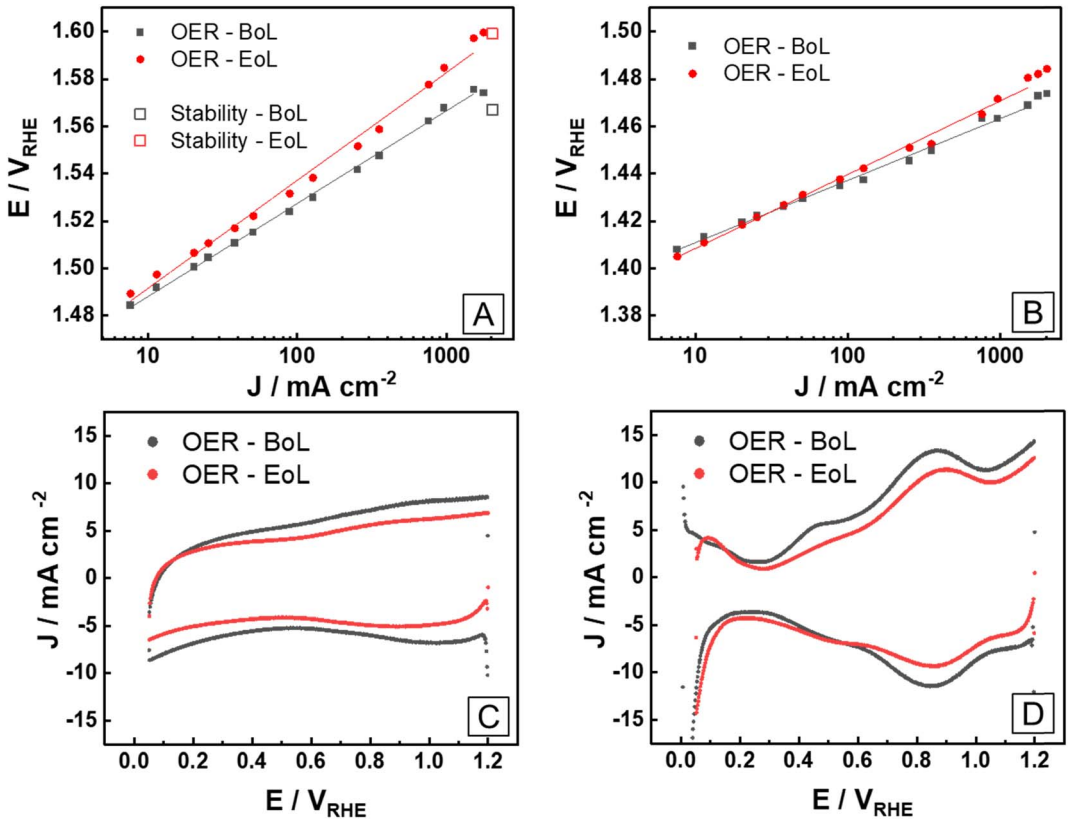

Fig. 5 OER activity and cyclic voltammetry recorded before (black) and after (red) the stability test for the IrO_x (A and C) and IrCo (B and D) self-supported catalysts. The OER step protocol, in filled symbols, was performed at room temperature for the IrO_x, and at 60 °C for the IrCo. In (A) the hollow symbols show 30 min of integrated measurements from the beginning (black) and end (red) of the stability test, see areas marked in Fig. 4A. In (C) and (D), the cyclic voltammograms were recorded at 100 mV s^{-1} between 0.05–1.2 V_{RHE} before the beginning-of-life (BoL) and after the end-of-life (EoL) OER activity measurements.

beginning and end of the stability measurement, see Fig. 4A, were integrated and plotted in hollow symbols together with the OER data in Fig. 5A. These recorded potentials closely match the trend of the OER protocol, showing that the stability measurements in the PTE setup are also capable of displaying the real performance of the catalyst in artifact-free data intervals. Furthermore, comparing the cyclic voltammogram features before and after the stability test, see Fig. 5C, the decrease in the double layer capacity strongly suggests a loss of surface area from the catalyst degradation process during the stability, which could have also been a contributing factor to the gradual increase in HFR during the stability measurement.

Despite the larger surface area of the Ir–Co catalyst in comparison to IrO_x, as seen in the cyclic voltammogram features in Fig. 5D, an analogous reduction in double-layer capacity was observed between beginning-of-life and end-of-life states following the stability test. While the Ir–Co catalyst did experience a Tafel slope reduction of 13 mV dec^{-1} between the beginning-of-life and end-of-life states, along with a decrease in activity at high current densities, it surprisingly exhibited an enhancement in its OER activity within the low current density range, as depicted in Fig. 5B. An explanation for this behavior could be the kinetic activation process of the microporous catalyst layer, which exhibits a mixed metallic and oxide nature.[28,37,38] This interpretation is further supported by

Table 3 Summary of OER activity in the beginning-of-life (BoL) and end-of-life (EoL) states of the IrO_x and Ir–Co catalyst in the PTE setup from the galvanostatic steps and integrated 30 minute intervals from the stability test of the IrO_x (indicated in black rectangles in Fig. 4A)

		Tafel slope (mV dec^{-1})		Potential (V_{RHE}@2 A cm_{geo}^{-2})	
Measurement state	Data source	IrO_x	Ir–Co	IrO_x	Ir–Co
BoL	Step OER	39	27	1.57	1.47
	2 A cm_{geo}^{-2} stability (30 min)	—	—	1.56	—
EoL	Step OER	45	36	1.59	1.48
	2 A cm_{geo}^{-2} stability (30 min)	—	—	1.59	—

the cyclic voltammogram features, see Fig. 5D, where distinct H_{upd} regions indicate remaining metallic Ir while the large capacitances are found in higher potentials suggesting the formation of oxides. Most interestingly, the remarkable performances observed using the self-supported catalyst preparation on PTEs have also been recently reported using a similar method in a membrane electrode assembly configuration.[39] The main electrochemical results are summarized in Table 3 below.

4. Conclusions

With this study, we have demonstrated the possibility of measuring OER potentials at relevant current densities >2 A cm^{-2} and temperatures with an improved configuration of the original GDE three-electrode half-cell that extends the range of application to conditions found in membrane electrode assemblies. By combining the PTE setup with PVD-based catalyst production, we demonstrate that it is possible to simplify and fast-track catalyst research closer to the industry standards at a lab scale. Although the results of the stability test should not necessarily provide a quantitative measure of catalyst degradation, they show the potential of the PTE setup to perform electrochemical tests under realistic high-current density conditions. Comparing the behavior of a IrO_x to a Ir–Co catalyst, the importance of employing measurement setups capable of attaining relevant current densities becomes particularly evident when considering the nonlinear evolution of the OER activity in nanostructured bimetallic catalysts.[19] Further development of the PTE setup in combination with parallel developments of this cell design[29] will unlock further capabilities such as pressurized and high-temperature measurements and coupling with online spectrometric analytics (ICP-MS, OES) to make quantitative degradation studies possible.

Author contributions

Pablo Collantes Jiménez: methodology, investigation, writing – original draft. Gustav K. H. Wiberg: conceptualization, methodology. Gustav Sievers: writing – review & editing, supervision, conceptualization. Volker Brüser: supervision, methodology. Matthias Arenz: writing – review & editing, supervision, conceptualization, all authors checked and approved the final version of the manuscript.

Conflicts of interest

Gustav Sievers has patent DE102016013185B4 issued to himself and Gustav Sievers and Pablo Collantes have PCT/EP2022/082 349 and EP 4 184 618 A1 issued to INP Greifswald.

Acknowledgements

The authors gratefully acknowledge the financial support by the German Federal Ministry of Education and Research (BMBF) in the framework of the VIP + Projekt. 03VP06451 (3DNanoMe).

References

1 W. T. Hong, M. Risch, K. A. Stoerzinger, A. Grimaud, J. Suntivich and Y. Shao-Horn, Toward the rational design of non-precious transition metal oxides for oxygen electrocatalysis, *Energy Environ. Sci.*, 2015, **8**, 1404–1427, DOI: 10.1039/c4ee03869j.

2 R. R. Rao, M. J. Kolb, N. B. Halck, A. F. Pedersen, A. Mehta, H. You, K. A. Stoerzinger, Z. Feng, H. A. Hansen, H. Zhou, L. Giordano, J. Rossmeisl, T. Vegge, I. Chorkendorff, I. E. L. Stephens and Y. Shao-Horn, Towards identifying the active sites on RuO2(110) in catalyzing oxygen evolution, *Energy Environ. Sci.*, 2017, **10**, 2626–2637, DOI: 10.1039/c7ee02307c.

3 C. Spöri, C. Brand, M. Kroschel and P. Strasser, Accelerated Degradation Protocols for Iridium-Based Oxygen Evolving Catalysts in Water Splitting Devices, *J. Electrochem. Soc.*, 2021, **168**, 034508, DOI: 10.1149/1945-7111/abeb61.

4 M. Bernt, A. Siebel and H. A. Gasteiger, Analysis of Voltage Losses in PEM Water Electrolyzers with Low Platinum Group Metal Loadings, *J. Electrochem. Soc.*, 2018, **165**, F305–F314, DOI: 10.1149/2.0641805jes.

5 A. Weiß, A. Siebel, M. Bernt, T.-H. Shen, V. Tileli and H. A. Gasteiger, Impact of Intermittent Operation on Lifetime and Performance of a PEM Water Electrolyzer, *J. Electrochem. Soc.*, 2019, **166**, F487–F497, DOI: 10.1149/2.0421908jes.

6 H. A. El-Sayed, A. Weiß, L. F. Olbrich, G. P. Putro and H. A. Gasteiger, OER Catalyst Stability Investigation Using RDE Technique: A Stability Measure or an Artifact?, *J. Electrochem. Soc.*, 2019, **166**, F458–F464, DOI: 10.1149/2.0301908jes.

7 A. Hartig-Weiss, M. F. Tovini, H. A. Gasteiger and H. A. El-Sayed, OER Catalyst Durability Tests Using the Rotating Disk Electrode Technique: The Reason Why This Leads to Erroneous Conclusions, *ACS Appl. Energy Mater.*, 2020, **3**, 10323–10327, DOI: 10.1021/acsaem.0c01944.

8 P. Aßmann, A. S. Gago, P. Gazdzicki, K. A. Friedrich and M. Wark, Toward developing accelerated stress tests for proton exchange membrane electrolyzers, *Curr. Opin. Electrochem.*, 2020, **21**, 225–233, DOI: 10.1016/j.coelec.2020.02.024.

9 M. Fathi Tovini, A. Hartig-Weiß, H. A. Gasteiger and H. A. El-Sayed, The Discrepancy in Oxygen Evolution Reaction Catalyst Lifetime Explained: RDE vs MEA - Dynamicity within the Catalyst Layer Matters, *J. Electrochem. Soc.*, 2021, **168**, 014512, DOI: 10.1149/1945-7111/abdcc9.

10 K.-R. Yeo, K.-S. Lee, H. Kim, J. Lee and S.-K. Kim, A highly active and stable 3D dandelion spore-structured self-supporting Ir-based electrocatalyst for proton exchange membrane water electrolysis fabricated using structural reconstruction, *Energy Environ. Sci.*, 2022, **15**, 3449–3461, DOI: 10.1039/D2EE01042A.

11 Z.-Y. Wu, F.-Y. Chen, B. Li, S.-W. Yu, Y. Z. Finfrock, D. M. Meira, Q.-Q. Yan, P. Zhu, M.-X. Chen, T.-W. Song, Z. Yin, H.-W. Liang, S. Zhang, G. Wang and H. Wang, Non-

iridium-based electrocatalyst for durable acidic oxygen evolution reaction in proton exchange membrane water electrolysis, *Nat. Mater.*, 2023, **22**, 100–108, DOI: **10.1038/s41563-022-01380-5**.

12 J. W. D. Ng, M. Tang and T. F. Jaramillo, A carbon-free, precious-metal-free, high-performance O2 electrode for regenerative fuel cells and metal-air batteries, *Energy Environ. Sci.*, 2014, **7**, 2017–2024, DOI: **10.1039/c3ee44059a**.

13 S. Nösberger, J. Du, J. Quinson, E. Berner, A. Zana, G. K. H. Wiberg and M. Arenz, The gas diffusion electrode setup as a testing platform for evaluating fuel cell catalysts: A comparative RDE-GDE study, *Electrochem. Sci. Adv.*, 2023, **3**, 1–12, DOI: **10.1002/elsa.202100190**.

14 T. Lazaridis, B. M. Stühmeier, H. A. Gasteiger and H. A. El-Sayed, Capabilities and limitations of rotating disk electrodes versus membrane electrode assemblies in the investigation of electrocatalysts, *Nat. Catal.*, 2022, **5**, 363–373, DOI: **10.1038/s41929-022-00776-5**.

15 S. Geiger, O. Kasian, M. Ledendecker, E. Pizzutilo, A. M. Mingers, W. T. Fu, O. Diaz-Morales, Z. Li, T. Oellers, L. Fruchter, A. Ludwig, K. J. J. Mayrhofer, M. T. M. Koper and S. Cherevko, The stability number as a metric for electrocatalyst stability benchmarking, *Nat. Catal.*, 2018, **1**, 508–515, DOI: **10.1038/s41929-018-0085-6**.

16 O. Kasian, S. Geiger, K. J. J. Mayrhofer and S. Cherevko, Electrochemical On-line ICP-MS in Electrocatalysis Research, *Chem. Rec.*, 2019, **19**, 2130–2142, DOI: **10.1002/tcr.201800162**.

17 J. Knöppel, S. Zhang, F. D. Speck, K. J. J. Mayrhofer, C. Scheu and S. Cherevko, Time-resolved analysis of dissolution phenomena in photoelectrochemistry – A case study of WO3 photocorrosion, *Electrochem. Commun.*, 2018, **96**, 53–56, DOI: **10.1016/J.ELECOM.2018.09.008**.

18 J. Knöppel, M. Möckl, D. Escalera-López, K. Stojanovski, M. Bierling, T. Böhm, S. Thiele, M. Rzepka and S. Cherevko, On the limitations in assessing stability of oxygen evolution catalysts using aqueous model electrochemical cells, *Nat. Commun.*, 2021, **12**, 2231, DOI: **10.1038/s41467-021-22296-9**.

19 K. Ehelebe, N. Schmitt, G. Sievers, A. W. Jensen, A. Hrnjić, P. Collantes Jiménez, P. Kaiser, M. Geuß, Y. P. Ku, P. Jovanovič, K. J. J. Mayrhofer, B. Etzold, N. Hodnik, M. Escudero-Escribano, M. Arenz and S. Cherevko, Benchmarking Fuel Cell Electrocatalysts Using Gas Diffusion Electrodes: Inter-lab Comparison and Best Practices, *ACS Energy Lett.*, 2022, **7**, 816–826, DOI: **10.1021/acsenergylett.1c02659**.

20 G. W. Sievers, A. W. Jensen, V. Brüser, M. Arenz and M. Escudero-Escribano, Sputtered Platinum Thin-films for Oxygen Reduction in Gas Diffusion Electrodes: A Model System for Studies under Realistic Reaction Conditions, *Surfaces*, 2019, **2**, 336–348, DOI: **10.3390/surfaces2020025**.

21 M. Inaba, A. W. Jensen, G. W. Sievers, M. Escudero-Escribano, A. Zana and M. Arenz, Benchmarking high surface area electrocatalysts in a gas diffusion electrode: Measurement of oxygen reduction activities under realistic conditions, *Energy Environ. Sci.*, 2018, **11**, 988–994, DOI: **10.1039/c8ee00019k**.

22 K. Ehelebe, D. Seeberger, M. T. Y. Paul, S. Thiele, K. J. J. Mayrhofer and S. Cherevko, Evaluating Electrocatalysts at Relevant Currents in a Half-Cell: The Impact of Pt Loading on Oxygen Reduction Reaction, *J. Electrochem. Soc.*, 2019, **166**, F1259–F1268, DOI: **10.1149/2.0911915jes**.

23 J. Schröder, V. A. Mints, A. Bornet, E. Berner, M. Fathi Tovini, J. Quinson, G. K. H. Wiberg, F. Bizzotto, H. A. El-Sayed and M. Arenz, The Gas Diffusion Electrode Setup as Straightforward Testing Device for Proton Exchange Membrane Water Electrolyzer Catalysts, *JACS Au*, 2021, **1**, 247–251, DOI: **10.1021/jacsau.1c00015**.

24 A. Bornet, R. Pittkowski, T. M. Nielsen, E. Berner, A. Maletzko, J. Schröder, J. Quinson, J. Melke, K. M. Ø. Jensen and M. Arenz, Influence of Temperature on the Performance of Carbon- and ATO-supported Oxygen Evolution Reaction Catalysts in a Gas Diffusion Electrode Setup, *ACS Catal.*, 2023, **13**, 7568–7577, DOI: **10.1021/acscatal.3c01193**.

25 T. Reier, M. Oezaslan and P. Strasser, Electrocatalytic oxygen evolution reaction (OER) on Ru, Ir, and Pt catalysts: A comparative study of nanoparticles and bulk materials, *ACS Catal.*, 2012, **2**, 1765–1772, DOI: **10.1021/cs3003098**.

26 S. Chatterjee, S. Intikhab, L. Profitt, Y. Li, V. Natu, R. Gawas and J. Snyder, Nanoporous Multimetallic Ir Alloys As Efficient And Stable Electrocatalysts For Acidic Oxygen Evolution Reactions, *J. Catal.*, 2021, **393**, 303–312, DOI: **10.30809/phe.1.2017.21**.

27 P. Jovanovič, N. Hodnik, F. Ruiz-Zepeda, I. Arčon, B. Jozinović, M. Zorko, M. Bele, M. Šala, V. S. Šelih, S. Hočevar and M. Gaberšček, Electrochemical Dissolution of Iridium and Iridium Oxide Particles in Acidic Media: Transmission Electron Microscopy, Electrochemical Flow Cell Coupled to Inductively Coupled Plasma Mass Spectrometry, and X-ray Absorption Spectroscopy Study, *J. Am. Chem. Soc.*, 2017, **139**, 12837–12846, DOI: **10.1021/jacs.7b08071**.

28 P. Collantes Jiménez, G. Sievers, A. Quade, V. Brüser, R. K. Pittkowski and M. Arenz, Gas diffusion electrode activity measurements of iridium-based self-supported catalysts produced by alternated physical vapour deposition, *J. Power Sources*, 2023, **569**, 232990, DOI: **10.1016/j.jpowsour.2023.232990**.

29 G. K. H. Wiberg, S. Nösberger and M. Arenz, Evolution of a GDE setup: Beyond ambient conditions, *Curr. Opin. Electrochem.*, 2022, **36**, 101129, DOI: **10.1016/j.coelec.2022.101129**.

30 H.-Y. Jung and J. W. Kim, Role of the glass transition temperature of Nafion 117 membrane in the preparation of the membrane electrode assembly in a direct methanol fuel cell (DMFC), *Int. J. Hydrogen Energy*, 2012, **37**, 12580–12585, DOI: **10.1016/j.ijhydene.2012.05.121**.

31 H. Mirsandi, W. J. Smit, G. Kong, M. W. Baltussen, E. A. J. F. Peters and J. A. M. Kuipers, Influence of wetting

conditions on bubble formation from a submerged orifice, *Exp. Fluids*, 2020, **61**, 83, DOI: 10.1007/s00348-020-2919-7.

32 C. Yu, P. Zhang, J. Wang and L. Jiang, Superwettability of Gas Bubbles and Its Application: From Bioinspiration to Advanced Materials, *Adv. Mater.*, 2017, **29**, 1703053, DOI: 10.1002/adma.201703053.

33 Q. Feng, X. Z. Yuan, G. Liu, B. Wei, Z. Zhang, H. Li and H. Wang, A review of proton exchange membrane water electrolysis on degradation mechanisms and mitigation strategies, *J. Power Sources*, 2017, **366**, 33–55, DOI: 10.1016/j.jpowsour.2017.09.006.

34 C. Liu, K. Wippermann, M. Rasinski, Y. Suo, M. Shviro, M. Carmo and W. Lehnert, Constructing a Multifunctional Interface between Membrane and Porous Transport Layer for Water Electrolyzers, *ACS Appl. Mater. Interfaces*, 2021, **13**, 16182–16196, DOI: 10.1021/acsami.0c20690.

35 C. Rakousky, G. P. Keeley, K. Wippermann, M. Carmo and D. Stolten, The stability challenge on the pathway to high-current-density polymer electrolyte membrane water electrolyzers, *Electrochim. Acta*, 2018, **278**, 324–331, DOI: 10.1016/j.electacta.2018.04.154.

36 C. Rakousky, U. Reimer, K. Wippermann, M. Carmo, W. Lueke and D. Stolten, An analysis of degradation phenomena in polymer electrolyte membrane water electrolysis, *J. Power Sources*, 2016, **326**, 120–128, DOI: 10.1016/j.jpowsour.2016.06.082.

37 A. Grimaud, A. Demortiere, M. Saubanere, W. Dachraoui, M. Duchamp, M. L. Doublet and J. M. Tarascon, Activation of surface oxygen sites on an iridium-based model catalyst for the oxygen evolution reaction, *Nat. Energy*, 2017, **2**, 17002, DOI: 10.1038/nenergy.2017.2.

38 M. Suermann, T. J. Schmidt and F. N. Büchi, Comparing the kinetic activation energy of the oxygen evolution and reduction reactions, *Electrochim. Acta*, 2018, **281**, 466–471, DOI: 10.1016/j.electacta.2018.05.150.

39 J. K. Lee, G. Anderson, A. W. Tricker, F. Babbe, A. Madan, D. A. Cullen, J. D. Arregui-Mena, N. Danilovic, R. Mukundan, A. Z. Weber and X. Peng, Ionomer-free and recyclable porous-transport electrode for high-performing proton-exchange-membrane water electrolysis, *Nat. Commun.*, 2023, **14**, 4592, DOI: 10.1038/s41467-023-40375-x.